MORPHOLOGY OF SPATIAL PATTERNS — POROUS MEDIA, SPINODAL DECOMPOSITION AND DISSIPATIVE STRUCTURES*

K.R. MECKE

Fachbereich Physik, Bergische Universität Wuppertal
D - 42097 Wuppertal, Germany

(Received January 15, 1997)

The morphological characterization of patterns is becoming more and more important in Statistical Physics as complex spatial structures now emerge in many systems. A suitable family of morphological measures, known in integral geometry as Minkowski functionals, characterize not only the connectivity but also the content and shape of spatial figures. The Minkowski functionals are related to familiar geometric measures: covered volume, surface area, integral mean curvature, and Euler characteristic. Integral geometry provides powerful theorems and formulae which makes the calculus convenient for many models of stochastic geometries, e.g. for the Boolean grain model. The measures are, in particular, applicable to random patterns which consist of non-regular, fluctuating domains of homogeneous phases on a mesoscopic scale. Therefore, we illustrate the integral geometric approach by applying the morphological measures to such diverse topics as porous media, chemical-reaction patterns, and spinodal decomposition kinetics: (A) The percolation threshold of porous media can be estimated accurately in terms of the morphology of the distributed pores. (B) Turing patterns observed in chemical reaction-diffusion systems can be analyzed in terms of morphological measures, which turn out to be cubic polynomials in the grey-level. We observe a symmetry-breaking of the polynomials when the type of pattern changes. Therefore, the morphological measures are useful order parameters to describe pattern transitions quantitatively. (C) The time evolution of the morphology of homogeneous phases during spinodal decomposition is described, focusing on the scaling behavior of the morphology. Integral geometry provides a means to define the characteristic length scales and to define the cross over from the early stage decomposition to the late stage domain growth.

PACS numbers: 02.40. +m, 81.35. +k, 05.70. Fh, 64.60. -i

* Presented at the IX Symposium on Statistical Physics, Zakopane, Poland, September 23–28, 1996.

1. Introduction

A large variety of complex spatial structures, *i.e.* patterns arise nowadays in many systems considered in Statistical Physics. For instance, Turing patterns in chemical reaction-diffusion systems (see Fig. 1(b)) and spatial structures of homogeneous phases evolving during spinodal decomposition (Fig. 1(c)) exhibit an enormous amount of information. Physical science faces the problem of reducing the spatial information to a finite number of relevant order parameters in order to find the dynamical equations or the governing laws of spatial structures. Also for the comparison of experiment and theory relevant quantities have to be identified. The morphology of the spatial structure plays an important role not only in porous media as shown in Fig. 1(a), where it determines physical properties such as percolation thresholds or diffusion coefficients, but also in many other composite materials the knowledge of spatial inhomogeneities is essential for an understanding of physical phenomena. As a rule, the bulk properties of a composite material depend on the chemistry and on the supramolecular morphology of its constituents. Therefore, the statistical theory should include geometrical as well as topological descriptors to characterize the size, shape and connectivity of the aggregating mesophases in such media.

Integral geometry provides mathematical means to describe spatial structures in a morphological way. This allows not only for a characterization of complex patterns and for a definition of spatial order parameters but also for the formulation of effective theories of mesophases on a mesoscopic scale in terms of geometric quantities.

Stochastic geometries are morphological structures in space which are not periodic or in anyway regular. They emerge whenever the process generating the spatial structure is random or too complex to describe it in an easy way. Consider for example a couple of needles thrown at random on a table or the distribution of oil droplets in an emulsion. The Boolean grain model generates random structures in space by overlapping bodies or 'grains' (*e.g.* spheres, rods, discs) each with arbitrary location and orientation. In this way the whole space is partitioned in covered and uncovered regions divided by pieces of the grain surfaces. In Fig. 1(a) a typical configuration is shown for 2-dimensional discs, that is used to simulate a porous medium. Although differences to realistic three-dimensional configurations are obvious some similarities in the morphological structure do occur.

Before I introduce the concepts of integral geometry and the Boolean grain model as an example of stochastic geometries let me first give some examples of patterns in physical systems and possible applications of morphological measures in Statistical Physics. The examples are considered in greater detail in Sec. 4.

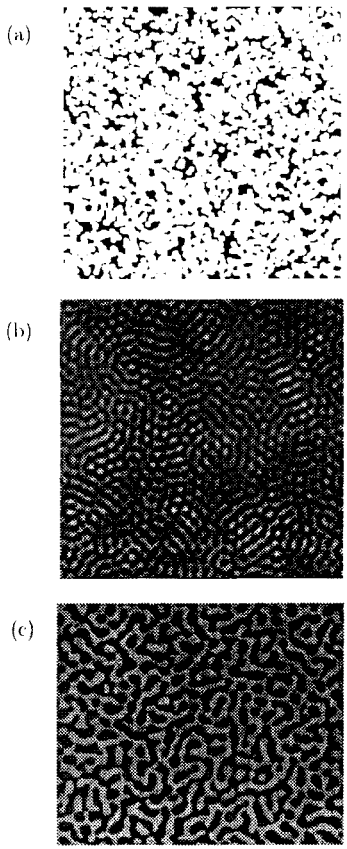

Fig. 1. Three examples of spatial patterns which have been studied extensively in recent years: (a) — A porous medium can be represented by overlapping balls distributed uniformly in space. Percolation is a typical physical phenomena addressed in such systems. Increasing the density of the pores, above a certain density threshold they form an infinite cluster spanning through the whole system, *i.e.* water can flow through the pores. How does the percolation threshold depend on the morphology of the pores? (b) — A turbulent pattern in a chemical reaction-diffusion system. Is there a unique way of characterizing the emerging structure, of distinguishing it from the regular Turing patterns, and of describing their transitions in a morphological way? (c) — Snapshot of spinodal decomposition kinetics. An homogeneous fluid phase separates instantaneously into an inhomogeneous distribution of coexisting liquid and vapor domains after quenching it into the spinodal region. The characteristic length scale grows with time, but does the morphology change with time too or does it scale?

1.1. Porous media

In Fig. 1 we show a sketch of a porous medium where pores (black regions) of different size and shape are distributed in a solid material (white region). For practical purposes one wants to know whether the pores percolate or not, *i.e.* if water can flow inside the pores through the system from the upper edge to the bottom. Generally, one observes a threshold in the density of the pores above which the system supports water flow. For densities below this threshold the pores do not percolate. Certainly, this threshold depends on the size and shape of the pores and on their statistical distribution. Therefore, we have to study the relevance of the morphology of the stochastic spatial structure on the percolation behavior. In Sec. 4.1 we calculate an estimate of the percolation threshold depending on the morphology of the pores. A final goal of this morphological approach is the description of macroscopic transport properties such as the diffusion constant of the material in terms of the morphology of the porous medium. In other words, an effective theory of porous media in terms of the morphology of the spatial structure [1,2].

1.2. Chemical reaction-diffusion patterns

A.M. Turing predicted in 1952 the existence of inhomogeneous spatial patterns in chemical reactions when diffusion of the species plays a role [3]. These patterns consist of regular and stationary spatially structured concentration profiles of the reactants. Thus, if diffusion is important the homogeneous solution of reaction-diffusion equations may become unstable and hexagonal patterns or stripes emerge. It was only in 1991 a group in Bordeaux followed by another in Austin could report the first experimental realization of such Turing patterns. Moreover, also a turbulent irregular and time-dependent pattern was found which is shown in Fig. 1(c). A pattern converts reversibly into another depending on system parameters, such as the temperature or the concentrations of the species. For example, defects occur in the hexagonal structure when the parameters are changed in such a way that the turbulent pattern becomes stable. Because of the proliferation of defects when the system is turning into the turbulent pattern, it is hard to tell whether the intermediate state of the pattern is hexagonal or turbulent already. The typical length scale or the correlation function do not change drastically [4]. Naturally, the question arises how one can describe irregular patterns in order to characterize the patterns in a unique way and, in particular, the transitions between them. There is a need to find measures which are capable to describe the morphology and topology of the patterns and which are sensitive to the transitions. In Sec. 4.2 we use the concepts of

morphological image analysis, in particular the morphological measures defined in integral geometry, to characterize the patterns and their transition in a unique way.

Introducing the concept of level contours the measures turn out to be polynomials of low order (cubic and fourth order) in the grey-scale level of the images. Thus the dependence on the experimental conditions is reflected only in a finite number of coefficients, which can be used as order parameters for the morphology of patterns. We observe a symmetry-breaking of the polynomials when the type of the pattern changes from hexagons to turbulence or stripes. Therefore it is possible to describe the pattern transitions quantitatively and it may be possible to classify them in a similar way to thermodynamic phase transitions.

1.3. Spinodal decomposition

Phase separation kinetics is probably the most common way of obtaining irregular spatial patterns on a mesoscopic scale. A fluid system above the critical temperature is usually homogeneous. But after a sudden quench below the critical point into the two-phase coexistence region the fluid separates into the coexisting liquid and vapor phase. Inside the spinodal regime the homogeneous fluid phase is unstable and thermal fluctuations in the density are growing instantaneously yielding an inhomogeneous distribution of vapor phase in liquid and the way around. One can distinguish two different time regimes in the process of phase separation: the early stage of spinodal decomposition kinetics and the late stage of domain growth. During the spinodal decomposition regime the density fluctuations grow and form finally homogeneous domains well separated by an interface. The typical length scale of these homogeneous domains of coexisting phases increases in the late stage driven by various mechanisms. A typical example of the pattern that emerges during spinodal decomposition in a two-dimensional liquid system is shown in Fig. 1(c).

The density correlation function from which one can extract the typical length scale, is the standard tool employed in describing the spatial structure of the system. However, it is not possible to obtain information about the morphology of the structure from the correlation function. The morphological measures introduced in Sec. 2.1 provide a mean to define not only the characteristic length scale but also to consider the time evolution of the morphology in a convenient and fast way. In particular, it is possible to define the cross over from the early stage decomposition to the late stage growth due to a change in the time dependence of the morphological measures.

1.4. General features

The patterns shown in Fig. 1 share the common features of complexity, randomness, and mesoscopic, which make integral geometry in particular important. One may formulate goals related to the application of morphological measures in Statistical Physics according to the common features of the patterns described above:

- **Complexity:** The spatial patterns are neither ordered nor structured in a simple way. Therefore, they can neither be characterized by the order parameters used for regular phases nor by usual means such as structure functions or defect statistics. It is necessary to reduce the information contained in a pattern and to find relevant measures as order parameters capable of describing spatial structures in a morphological way. For this purpose we introduce in Sec. 2 the Minkowski functionals as morphological measures for complex structures.
  Since physical phenomena in inhomogeneous systems depend on the morphology of the spatial structure one should be able to calculate physical properties in terms of relevant morphological measures. For instance, percolation thresholds and also transport coefficients, such as the diffusion constant, depend on the shape of the pores. In Sec. 4.1 we derive an estimate for the percolation threshold depending on the shape of the single pores.
- **Randomness:** The spatial structures are random in nature, *i.e.* the domains are fluctuating thermally or are generated by a stochastic process. Therefore, measures characterizing the shape should be applicable, accessible and calculable for various stochastic models. We present in Sec. 3 the Boolean grain model as a standard model for stochastic geometries.
  The typical method to describe the spatial structure of random systems is the structure function, namely the 2-point correlation function. However, in general this approach fails to characterize the geometric shape of the structures. Additionally it turned out that in many systems higher correlations are essential. Moreover, due to the small size of the systems it is often very difficult to obtain accurate structure functions. On the other hand, it might be time consuming to calculate them in large systems, for instance, in computer simulations of spinodal decomposition kinetics (Sec. 4.3). Thus there is a need for statistical measures which includes higher correlations, *i.e.* not only 2-point functions, and which are fast and reliable even in small systems, in order to characterize random structures in a morphological way.
- **Mesoscopic:** In general, the domain size of the patterns is larger than atomic lengths, typically several nanometers. Thus each domain

contains a large amount of molecules so that we must not look for a microscopic model but for an effective theory on a mesoscopic scale. In Ref. [14] we argue, for example, that on a mesoscopic scale the physics is governed by morphological thermodynamics formulated in terms of morphological measures.

The paper is organized as follows. In Sec. 2 we introduce the concepts of integral geometry in order to provide the mathematical tool to describe spatial structures in a morphological way. We define a complete family of morphological measures, the so-called Minkowski functionals, including the Euler characteristic as a prominent topological quantity.

Since most of the patterns considered in physical systems are stochastic in nature we introduce in Sec. 3 the Boolean grain model as a convenient way of generating stochastic geometries, *i.e.* spatial structures. The random patterns can be characterized by the morphological measures introduced in Sec. 2.1.

In Sec. 4 we apply the concepts of integral geometry and the Boolean grain model to various physical phenomena and in particular to the examples 1.1 — 1.3 mentioned above. The aim of this paper is neither to review these various topics nor to give a complete list of references. Also, it is not intended to cover every interesting phenomena within these fields but only to apply the concept of integral geometry and the notion of morphological measures to selected problems among them.

2. Integral geometry

Since the methods of integral geometry are not widely known among physicists in this section we compile some pertinent facts [5–7]. First, we introduce the Minkowski functionals as morphological measures of homogeneous domains, well known in digital picture analysis [8] and mathematical morphology [9]. We then proceed on to presenting the important theorems and the formulas for these measures which enables us to calculate, for example, mean values analytically in Sec. 3. Finally, we demonstrate with three examples the usefulness of the Minkowski functional for many applications in the field of Statistical Physics.

2.1. Morphological measures

First, we define what we want to call a morphological measure. Let us consider a homogeneous domain such as the ellipsoid shown in Fig. 2. Let the domain K be a compact convex set in $\mathbb{R}^d$. The class of closed bounded convex subsets of $\mathbb{R}^d$, *i.e.* domains, is denoted by $\mathcal{K}$. We consider patterns $A = \cup_i K_i$ resembled by compact convex sets $K_i \in \mathcal{K}$. Let $\mathcal{R}$ denote the

class of subsets of $\mathbb{R}^d$ that can be represented as a finite union of sets from $\mathcal{K}$, *i.e.* $A \in \mathcal{R}$ if and only if $A = \cup_{i=1}^{N} K_i$, $N < \infty$, $K_i \in \mathcal{K}$. The class $\mathcal{R}$ also includes the empty set $\emptyset$. An examples of such a type of pattern is a porous medium shown in Fig. 1(a). But the continuous patterns shown in Fig. 1(b) and (c) can also be decomposed in convex subsets. For instance, due to a finite resolution of the experimental equipment (b) or due to simulations on a lattice (c) one has often an underlying pixel structure. Each pixel (squares or hexagons in two dimensions) is a compact, convex set and the whole pattern is the union of all of these pixels. In Fig. 6 we show an example of such a lattice structure.

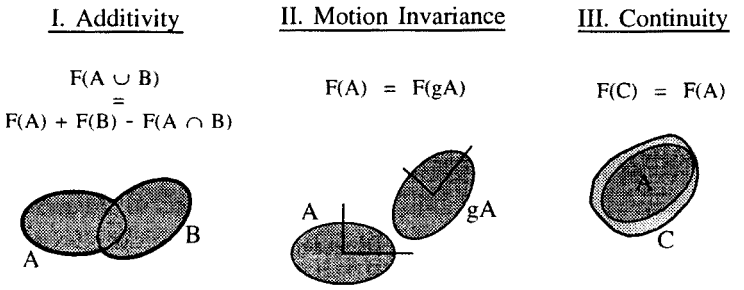

Fig. 2. The three defining properties of a morphological measure: The area $F(A)$ of a domain A, for instance, does not depend on the orientation and location of A (motion-invariance) and it changes continuously if A is approximated by another shape C. Furthermore the area $F(A \cup B)$ of the union of two domains A and B is additive with respect to the subtraction of the overlap $A \cap B$.

Let us now define three general properties a functional $\mathcal{W} : \mathcal{R} \to \mathbb{R}$ should possess in order to be a morphological measure:

(i) **Additivity:** The functional of the union $A \cup B$ of two domains $A, B \in \mathcal{R}$ is the sum of the functional of the single domains subtracted by the intersection

$$\mathcal{W}(A \cup B) = \mathcal{W}(A) + \mathcal{W}(B) - \mathcal{W}(A \cap B)\,. \tag{2.1}$$

This relation generalizes the common rule for the addition of the volume of two domains to the case of a morphological measure. The volume, *i.e.* the measure of the double-counted intersection has to be subtracted.

(ii) **Motion invariance:** Let $\mathcal{G}$ be the group of motions, namely translations and rotations in $\mathbb{R}^d$. The transitive action of $g \in \mathcal{G}$ on a domain $A \in \mathcal{R}$ is denoted by gA. Then

$$\mathcal{W}(gA) = \mathcal{W}(A)\,, \tag{2.2}$$

i.e. the morphological measure of a domain is independent of its location and orientation in space.

(iii) **Continuity:** If a sequence of convex sets $K_n \to K$ for $n \to \infty$, K_n, $K \in \mathcal{K}$ converges towards the convex set K (with convergence defined in terms of the Hausdorff metric for sets), then

$$\mathcal{W}(K_n) \to \mathcal{W}(K) . \tag{2.3}$$

Intuitively, this continuity property expresses the fact that an approximation of a convex domain by convex polyhedra K_n, for example, also yields an approximation of $\mathcal{W}(K)$ by $\mathcal{W}(K_n)$. We emphasize that we require this condition only for the morphological measure of convex sets $K \in \mathcal{K}$ and not for unions $A \in \mathcal{R}$.

In three-dimensional space we can give easily examples of morphological measures which obey the three conditions *(i)–(iii)*: for instance, the volume V and the surface area S of a domain in three dimensions are continuous, motion-invariant and additive. In two dimensions we mention the area F and the boundary length U of a domain as morphological measures in the sense described above.

Naturally the question arises if there are other measures which obey the conditions *(i)–(iii)* and if there is a systematic way to find such measures. In order to answer this question we introduce the Euler characteristic χ as a prominent member of the family of morphological measure.

2.2. The Euler characteristic χ

Since the Euler characteristic χ is not a widely used quantity we introduce here some useful relations. In two dimensions the Euler characteristic for a spatial set A is defined in algebraic topology by the difference of the number of connected components $\#_C$ and the number of holes $\#_H$, *i.e.*

$$\chi(A) = \#_C - \#_H . \tag{2.4}$$

Thus, the Euler characteristic of the pattern shown in Fig. 6 is zero, *i.e.* $\chi = 1 - 1 = 0$, because the configuration exhibits one connected black components and one white hole. The Gauß–Bonnet theorem states that this quantity equals the integral of the curvature κ along the boundary ∂A of A

$$\chi(A) = \frac{1}{2\pi} \int_{\partial A} dl\, \kappa(l) . \tag{2.5}$$

Thus, for a disc B_R of radius R one obtains $\kappa = 1/R$ and $\chi(B_R) = 1$ in accordance with Eq. (2.4). Similar definitions and relations hold in three

dimensions though distinction between two different kinds of holes must be made. The Euler characteristic is defined by the sum of the number of connected components $\#_C$ and the number of cavities $\#_K$ subtracted by the number of torus-like holes $\#_T$, *i.e.*

$$\chi(A) = \#_C - \#_T + \#_K \,. \tag{2.6}$$

Integral geometry [5,6] provides in the context of overlapping grains a more useful definition of χ. The Euler characteristic can be introduced first for convex sets $K \in \mathcal{K}$ by

$$\chi(K) = \begin{cases} 1 & , \quad K \in \mathcal{K}\,,\ K \neq \emptyset\,, \\ 0 & , \quad K = \emptyset\,. \end{cases} \tag{2.7}$$

and then extended to $\mathcal{R}$ via the additivity relation (2.1),

$$\chi(A \cup B) = \chi(A) + \chi(B) - \chi(A \cap B) \tag{2.8}$$

for any $A, B \in \mathcal{R}$. In particular, one finds for the union $\cup_{i=1}^{N} K_i$ of convex domains

$$\chi(\cup_{i=1}^{N} K_i) = \sum_i \chi(K_i) - \sum_{i<j} \chi(K_i \cap K_j) + \ldots \tag{2.9}$$

$$+(-1)^{N+1} \chi(K_1 \cap K_2 \cap \ldots \cap K_N)\,,$$

that follows from Eq. (2.8) by induction. The right hand side of Eq. (2.9) involves only convex sets and may be used together with Eq. (2.7) to compute $\chi(A)$ for any $A \in \mathcal{R}$, as illustrated in Fig. 3. We also note that $\chi : \mathcal{R} \to \mathbb{Z}$ is motion-invariant and it can be shown to agree with the Euler characteristic as defined in algebraic topology. In the physical literature the Euler characteristic is usually associated with the surface ∂A of a domain A. For closed $(d-1)$-dimensional surfaces in $\mathbb{R}^d$ one has the simple relationship

$$\chi(\partial A) = \chi(A) \left(1 + (-1)^{d-1}\right)\,, \tag{2.10}$$

especially $\chi(\partial A) = 2\chi(A)$ for $d = 3$. Since the Euler characteristic is constant and equal one for convex sets, it is also continuous as required by the condition (2.3). Therefore the Euler characteristic is a morphological measure in the sense given by the conditions *(i)-(iii)*.

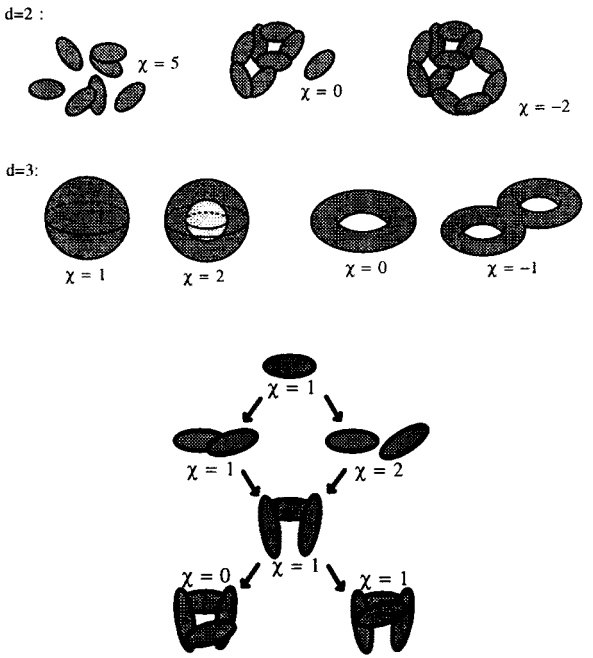

Fig. 3. Examples of the Euler characteristic for typical structures: in a two dimensional space the Euler characteristic $\chi = \#_C - \#_H$ is equal to the difference of connected components $\#_C$ and holes $\#_H$. In three dimensions ($d = 3$) one has to distinguish between cavities $\#_K$ (which count positive) and torus-like holes $\#_T$ (counting negative) in order to obtain Euler's formula $\chi = \#_C - \#_T + \#_K$. Generally, negative Euler characteristics indicate netlike structures. Using the additivity relation (2.8) one can calculate the Euler characteristic recursively for any configuration of overlapping shapes.

2.3. Minkowski functionals

Now we are able to define the Minkowski functionals for domains $A \in \mathcal{R}$ by

$$W_\nu(A) = \int \chi(A \cap E_\nu) d\mu(E_\nu) \quad , \quad \nu = 0, \ldots, d-1 \tag{2.11}$$

and $W_d(A) = \omega_d \chi(A)$. Here, E_ν is an $\nu-$dimensional plane in $\mathbb{R}^d$. The integral runs over all positions (induced by translations and rotations) of E_ν, weighted with the so-called kinematical density $d\mu(E_\nu)$ [5,6] which is related to the invariant Haar measure on the group of motions $\mathcal{G}$ and is normalized such that for a d-dimensional ball B_R of radius R, $W_\nu(B_R) = \omega_d R^{d-\nu}$. The volume of the unit ball $\mathrm{V}(B_{R=1})$ is $\omega_d = \pi^{d/2}/\Gamma(1 + d/2)$, namely

$\omega_1 = 2$, $\omega_2 = \pi$, and $\omega_3 = 4\pi/3$. Sometimes it is convenient to normalize the functionals

$$M_\nu(A) = \frac{\omega_{d-\nu}}{\omega_\nu \omega_d} W_\nu(A)\,, \quad \nu = 0, \ldots, d\,. \tag{2.12}$$

In $d = 3$, for instance, one obtains for balls of radius R

$$M_0 = \frac{4\pi}{3}R^3\,, \quad M_1 = \frac{\pi}{2}R^2\,, \quad M_2 = \frac{2}{\pi}R\,, \quad M_3 = \frac{3}{4\pi}\,. \tag{2.13}$$

The definition (2.11) of the Minkowski functionals is a generalization of the common determination of the volume $V = W_0(A)$ of a domain A by the integral

$$W_0(A) = \int\limits_{\mathbb{R}^d} I_A(\vec{x})\, d\vec{x} \tag{2.14}$$

over the characteristic function

$$I_A(\vec{x}) := \chi(A \cap \vec{x}) = \begin{cases} 1 & \text{if } \vec{x} \in A \\ 0 & \text{if } \vec{x} \notin A \end{cases}\,. \tag{2.15}$$

The volume W_0 equals the number of possible intersections of a point $\vec{x}$ with the domain A. Generally, the functionals $W_\nu(A)$ count the possible intersections of ν-dimensional planes with the domain A.

We are primarily interested in the two- and three-dimensional cases, where the Minkowski functionals are related to familiar measures, *i.e.* the functionals M_ν can be expressed in well-known geometric terms for $d \leq 3$. In particular, in a three-dimensional space the family of Minkowski functionals consists of the Euler characteristic χ, the covered volume V, the surface area F of the coverage, and its integral mean curvature H, *i.e.*

$$\begin{aligned} W_0(K) &= V(K)\,, & 3W_1(K) &= F(K)\,, \\ 3W_2(K) &= H(K)\,, & 3W_3(K) &= 4\pi\chi(K)\,. \end{aligned} \tag{2.16}$$

In two-dimensional space we obtain the Euler characteristic χ, the covered area F, and the boundary length U of the coverage, *i.e.*

$$F = W_0\,, \quad U = 2W_1\,, \quad \chi = \frac{1}{\pi}W_2\,. \tag{2.17}$$

According to the definition (2.11), the Minkowski functionals on $\mathcal{R}$ inherit from the Euler characteristic the property of additivity, *i.e.*

$$W_\nu(A \cup B) = W_\nu(A) + W_\nu(B) - W_\nu(A \cap B)\,, \tag{2.18}$$

as well as motion-invariance. These features together with their "conditional continuity" (the W_ν are continuous when restricted to $\mathcal{K}$) specify the Minkowski functionals as morphological measures, *i.e.* as a distinguished family of geometrical and topological descriptors.

We emphasize that the Minkowski functional W_ν is homogeneous of order $d-\nu$, *i.e.* for a dilated domain λA one obtains

$$W_\nu(\lambda A) = \lambda^{d-\nu} W_\nu(A)\,. \tag{2.19}$$

This relation enables us, for instance, to extract a time-dependent scaling length from the morphological measures in the case of spinodal decomposition considered in Sec. 4.3.

One can calculate explicit expressions for the Minkowski functionals for various domains in $\mathbb{R}^d$, namely for an j-dimensional ball B_ρ^j of radius ρ, with $d \geq j \geq d-\nu$,

$$W_\nu(B_\rho^j) = \frac{\binom{\nu+j}{d}}{\binom{\nu+j}{j}} \frac{\omega_\nu \omega_j}{\omega_{\nu+j-d}} \rho^{d-\nu}\,, \tag{2.20}$$

an j-dimensional cuboid Q_ρ^j with edge length ρ,

$$W_\nu(Q_\rho^j) = \frac{\binom{\nu+j}{d}}{\binom{\nu+j}{j}} \omega_\nu \rho^{d-\nu}\,, \tag{2.21}$$

a d-dimensional cylinder Z^d of radius ρ and height h,

$$W_\nu(Z^d) = \frac{\omega_{d-1}}{d} \left(\frac{\nu \omega_\nu}{\omega_{\nu-1}} \rho^{d-\nu} + (d-\nu) h \rho^{d-\nu-1} \right)\,. \tag{2.22}$$

Originally the Minkowski functionals derive from the theory of convex sets and therefore many theorems are restricted to the class $\mathcal{K}$ of convex domains. Nevertheless, the extension to unions of convex sets can be achieved in the described way using the Euler characteristic as starting point [5]. Then we can apply these measures to investigate the spatial pattern of coverage models, as described in the introduction, by taking the values for single convex shapes (ball or cube, for instance) and using the additivity relation (2.18) in order to calculate them for the more complex, non-convex patterns shown in Figs 1(a)–(c).

The definition of morphological measures by integrals over the motion of ν-dimensional planes is unusual but nevertheless very instructive and convenient. A different approach to Minkowski functionals starts with the well known differential geometry of surfaces. Minkowski functionals generalize curvature integrals over smooth surfaces to the case of surfaces with singular edges and corners. In the example of the covering shown in Fig. 1(a)

such irregularities arise from the intersections of the overlapping balls. Let A be a compact domain in $\mathbb{R}^d$ with *regular* boundary $\partial A \in \mathcal{C}^2$ and $d-1$ principal radii of curvature R_i $(i = 1, \ldots d-1)$. The functionals $W_\nu(A)$, with $\nu \geq 1$, can be defined by the surface integrals

$$W_{\nu+1}(A) = \frac{1}{(\nu+1)\binom{d}{\nu+1}} \int S_\nu(\frac{1}{R_1}, \ldots, \frac{1}{R_{d-1}}) d\mathcal{O}, \tag{2.23}$$

where S_ν denotes the ν-th elementary symmetric function and $d\mathcal{O}$ the $(d-1)$-dimensional surface element [5, 6]. Especially in three dimensions one obtains

$$W_1 = \frac{1}{3}\int d\mathcal{O}, \quad W_2 = \frac{1}{3}\int H d\mathcal{O}, \quad W_3 = \frac{1}{3}\int G d\mathcal{O} \tag{2.24}$$

with the Gaussian

$$G = \frac{1}{R_1 R_2} \tag{2.25}$$

and the mean curvature

$$H = \frac{1}{2}\left(\frac{1}{R_1} + \frac{1}{R_2}\right). \tag{2.26}$$

One disadvantage of this differential geometric approach to the Minkowski functionals is the need of 'smooth' surfaces in contrast to the definition given by Eq. (2.11). However, one can avoid the condition of smooth surfaces by using the concept of the parallel body K_ε of a convex grain K, *i.e.* the convex domain K_ε parallel to K at a distance ε:

$$K_\varepsilon := \cup_{x \in K} B_\varepsilon(x). \tag{2.27}$$

Thus, the parallel body K_ε consists of all points within a distance smaller than ε from the domain K. For a convex domain with a piece wise smooth boundary like a polyhedron the parallel body K_ε is sufficient smooth and therefore we can perform the surface integral (2.23). Using the continuity relation (2.3) of $W_\nu(K_\varepsilon)$ one can define the Minkowski functionals W_ν for K by

$$W_\nu(K) := \lim_{\varepsilon \to 0} W_\nu(K_\varepsilon), \tag{2.28}$$

i.e. by surface integrals of curvatures on the parallel body K_ε. Thus, the continuity (2.3) of the functionals W_ν allows the definition of integrals of the curvature functions S_ν even for surfaces with singular edges, *i.e.* the Minkowski functionals generalize curvatures as differential geometric quantities to singular edges. Therefore, it is straightforward to apply the notion of morphological measures even to patterns consisting of lattice cells (see the example shown in Fig. 6).

2.4. Theorems and formulas

A remarkable theorem in integral geometry is the completeness of the Minkowski functionals [5]. The theorem asserts that any additive, motion-invariant and conditional continuous functional $\mathcal{W}(A)$ on subsets $A \subset \mathbb{R}^d$, $A \in \mathcal{R}$, *i.e.* each morphological measure is a linear combination of the $d+1$ Minkowski functionals,

$$\mathcal{W}(A) = \sum_{\nu=0}^{d} c_\nu W_\nu(A)\,, \tag{2.29}$$

with real coefficients c_ν independent of A. Thus, every morphological measure $\mathcal{W}$ defined by the properties (2.1)–(2.3) can be written in terms of Minkowski functionals W_ν. In other words, the Minkowski functionals are the complete set of morphological measures. In a d-dimensional ambient space, the curvature integrals (2.23) constitute the distinct family of $d+1$ morphological measures which share the common features of being additive, motion-invariant and continuous. In $d=3$ they are related to familiar measures: covered volume, surface area, integral mean curvature and Euler characteristic.

An important consequence of this theorem is the possibility to calculate analytically certain integrals of Minkowski functionals. The "principal kinematical formulae", for instance, describe the factorization of the Minkowski functionals of the intersection $A \cap B$ of two shapes A and B if one integrates over the motions, namely the translations and rotations of one of them. The kinematical formulae may be written concisely in the form

$$\int_{\mathcal{G}} M_\nu(A \cap gB)dg = \sum_{\mu=0}^{\nu} \binom{\nu}{\mu} M_{\nu-\mu}(B) M_\mu(A)\,. \tag{2.30}$$

The integral is performed with respect to the invariant Haar measure dg of the group of motions $\mathcal{G}$ and runs over all motions gB of the set B, with $A, B \in \mathcal{R}$. The proof of this formula is straightforward so we can give a short sketch. The integral $I_\nu(A,B) = \int_{\mathcal{G}} W_\nu(A \cap gB)dg$ is a motion-invariant, additive and conditional continuous functional for the grain A as well as for B. Thus one can find a representation

$$I_\nu(A,B) = \sum_{\mu,\lambda} c^\nu_{\mu\lambda} W_\mu(A) W_\lambda(B) \tag{2.31}$$

with some coefficients $c^\nu_{\mu\lambda}$. As $I_\nu(A,B)$ is homogeneous of order $2d-\nu$ the coefficients obey the constraint $c^\nu_{\mu\lambda} = c^\nu_\mu \delta_{\nu-\mu-\lambda}$ with the Kronecker-symbol

$\delta_i = 0, 1$ if $i = 0$ resp. $i \neq 0$. For the calculation of the remaining constants I refer to Ref. [5]. It is sufficient to calculate the integral for specified situations as c_μ^ν does not depend on A and B.

In particular, the kinematical formulae (2.30) include the formula for the factorization of the volume W_0 due to the motion of the grains,

$$\int_{\mathcal{G}} W_0(A \cap gB)dg = W_0(A)W_0(B)\,. \tag{2.32}$$

The kinematical formulae (2.30) describes the factorization of the Minkowski functionals $W_\nu(A \cap gB)$ of the intersection of two grains in the Minkowski functionals $W_\nu(A)$ and $W_\nu(B)$ of the single grains. This is an immediate consequence of the completeness theorem and would be in contrast extremely hard to prove it using elementary integration theory. Even the calculation of the factorization (2.32) of the volume W_0 for some simple shapes would fill up pages. This factorization caused by the motion of the grains will be used for the calculation of mean values of the Minkowski functionals in Chapter 3.

The kinematical formulae (2.30) are useful mathematical tools in stereology and stochastic geometry. The Minkowski functionals can be calculated efficiently for any given coverage without requiring statistical assumptions about the underlying point set. Moreover, mean values can be calculated exactly for the classical Boolean model [10], where the centers of balls are distributed in $\mathbb{R}^d$ according to Poisson's law, which is often employed as a reference model. This will be done in the next section.

3. Stochastic geometry

Integral geometry is concerned with the morphology and motion of single grains. This was considered in the previous section. Now we want to study the properties, in particular the morphological measures of many randomly distributed objects, for instance, holes in a porous medium.

Stochastic geometry is the mathematical frame that concerns such random structures. In particular it formulates mathematical models for the description and give proofs about the existence and uniqueness of mean values or variances. Since 1975 - possibly the beginning of modern stochastic geometry due to the works of Harding and Kendall (1974), as well as Matheron (1975) — a fast growing amount of literature has been published [11–13]. Here, I consider only one specific model, namely the Boolean grain model [14].

The Boolean model (Poisson-grain model, germ-grain model) starts with independently and random distribution of points x_i (germs) in the Euclidean space $\mathbb{R}^d$. We assume an homogeneous density ρ of points in a convex domain

$\Omega \subset \mathbb{R}^d$ (homogeneous Poisson point process). At every point x_i we fix identical but independent oriented convex bodies K_i (grains).

To introduce the kind of calculation usually done in the Boolean grain model we calculate the mean value of the covered volume: A configuration of the model is given by the union $\mathcal{A} = \cup_i K_i$ of convex grains K_i with volume $V := W_0(K_i)$. The average over all possible configuration is equal to an integral over the positions and orientations of every grain independent on the position and orientation of the others. This corresponds to a Poissonian distribution of the grains. The mean value $v(\rho)$ of the covered volume $V(\mathcal{A})$ per volume $|\Omega|$ of a test domain $\Omega \subset \mathbb{R}^d$ can be obtained immediately by the average $< \chi(\mathcal{A} \cap \vec{x}) >$ of incidence at a fixed point $\vec{x} \in \Omega$ in the test domain. Here we assume explicitly an homogeneous distribution of grains and consider only such translated grains gK_i which have a non-empty intersection $gK_i \cap \Omega \neq \emptyset$. Using the decomposition of the Euler characteristic

$$\chi(\mathcal{A}, \vec{x}) = \chi(\mathcal{A} \cap \vec{x}) = 1 - \prod_{i=1}^{N} (1 - \chi(K_i \cap \vec{x})) \tag{3.1}$$

one obtains immediately for the mean value of the covered volume

$$\begin{aligned} v(\rho) &= \langle \chi(\mathcal{A} \cap \vec{x}) \rangle = 1 - \prod_{i=1}^{N} \langle 1 - \chi(K_i \cap \vec{x}) \rangle \\ &= 1 - \left(1 - \frac{W_0(K)\rho}{N}\right)^N \longrightarrow_{N \to \infty} 1 - \mathrm{e}^{-\rho V}, \end{aligned} \tag{3.2}$$

where the average $\chi(K_i \cap \vec{x})$ over a single grain yields the volume $W_0(K_i) = V$ and the density $\rho = |\Omega|/N$ is given by the volume $|\Omega|$ and the number N of grains. The mean volume $1 - v(\rho) = \mathrm{e}^{-\rho V(K)} = P_0(K)$ of the uncovered region in space corresponds to the probability $P_0(K)$ that no point of a point process lies inside the given region K of a single grain. This so-called 'void probability function' of the point process possesses this simple expression only for Poisson distributed points.

In contrast to the mean value of the volume W_0 the other Minkowski functionals W_i are not related to an probability measure and cannot be represented by a function $\langle \chi(\mathcal{A} \cap \vec{x}) \rangle$ which is easily decomposable. Therefore, we propose another approach to calculate mean values by taking into account only the additivity (2.18) of the Minkowski functionals.

To be as rigorous as possible and desirable we recapitulate definitions and notations. We consider N grains $K_i \in \mathcal{K}$, $i = 1, \ldots, N$ out of the convex ring $\mathcal{K}$. We assume that their Minkowski functionals $M_\nu(K_i)$ are finite but not necessary equal and that we can define a mean value $m_\nu = \langle M_\nu(K_i) \rangle$

averaged over all shapes. Throughout this section we use for simplicity the normalization $M_\nu = (\omega_{d-\nu}/\omega_d\omega_\nu)W_\nu$ of the functionals W_ν (see Eq. (2.12)). At a given point $\vec{x} \in K_i$ of each grain (the germ or center) we fix a d-frame to determine besides the position $\vec{x}_i$ of the grain K_i its orientation. These so marked penetrable grains are placed independently at N random sites in a d-cube Ω with random isotropic orientation of their d-frames. To avoid edge effects we use periodic boundary conditions on $\partial\Omega$. Thus, a random configuration of grains gives rise to a set

$$\mathcal{A}_N = \bigcup_{i=1}^{N} g_i K_i \in \mathcal{K}\,. \tag{3.3}$$

Our aim is to compute the mean value of $M(\mathcal{A}_N)$, where the configurational average is done with the product density element

$$d\mu(g_1\,,\ldots,g_N) = \frac{1}{|\Omega|^N}\prod_{i=1}^{N} dg_i\,, \tag{3.4}$$

with $\int dg_i = |\Omega| = V(\Omega)$. The integration over translations is restricted to Ω, *i.e.* the translated grains should have a non-empty intersection with Ω.

Consider first the configurational average for a single grain, K_N. Additivity of $M_\nu(A)$ (see 2.18) combined with the kinematical formula (2.30) and with the motion-invariance $M_\nu(g_N K_N) = M_\nu(K_N)$ leads to

$$\begin{aligned}
&\int M_\nu(\mathcal{A}_N)\frac{dg_N}{|\Omega|} \\
&\quad = M_\nu(\mathcal{A}_{N-1}) + M_\nu(K_N) - \int M_\nu(\mathcal{A}_{N-1}\cap g_N K_N)\frac{dg_N}{|\Omega|} \\
&\quad = M_\nu(\mathcal{A}_{N-1}) + M_\nu(K_N) - \sum_{\mu=0}^{\nu}\binom{\nu}{\mu} M_{\nu-\mu}(\mathcal{A}_{N-1})M_\mu(K_N)\,.
\end{aligned} \tag{3.5}$$

The further average over size and shape of K_N replaces $M_\nu(K_N)$ by its mean value, m_ν. Since the grains are independently and identically distributed in location, orientation, size and shape, Eq. (3.5) leads to a simple difference equation for the mean value $\bar{M}_\nu(N) = \langle M_\nu(\mathcal{A}_N)\rangle$,

$$\bar{M}_\nu(N) - \bar{M}_\nu(N-1) = m_\nu - \sum_{\mu=0}^{\nu}\binom{\nu}{\mu}\bar{M}_{\nu-\mu}(N-1)m_\mu\,. \tag{3.6}$$

In the limit $N, \Omega \to \infty$, $\rho = N/|\Omega|$ fixed one obtains a system of differential equations

$$\frac{\partial m_\nu(\rho)}{\partial\rho} = m_\nu - \sum_{\mu=0}^{\nu}\binom{\nu}{\mu} m_{\nu-\mu}(\rho)m_\mu\,. \tag{3.7}$$

for the normalized mean values

$$m_\nu(\rho) = \lim_{N\to\infty} \frac{\bar{M}_\nu(N)}{|\Omega|} . \tag{3.8}$$

One can solve recursively the differential equations (3.7) yielding the mean values for the Minkowski functionals

$$\begin{aligned} m_0(\rho) &= 1 - \mathrm{e}^{-\rho m_0} , \\ m_1(\rho) &= \rho m_1 \, \mathrm{e}^{-\rho m_0} , \\ m_2(\rho) &= (\rho m_2 - m_1^2 \rho^2) \, \mathrm{e}^{-\rho m_0} , \\ m_3(\rho) &= (\rho m_3 - 3 m_1 m_2 \rho^2 + m_1^3 \rho^3) \, \mathrm{e}^{-\rho m_0} . \end{aligned} \tag{3.9}$$

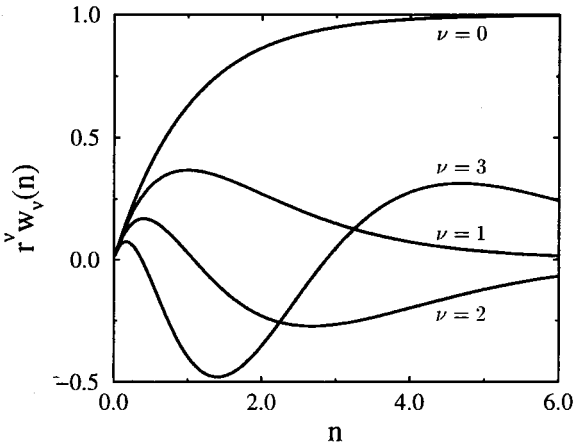

Fig. 4. The mean value of the Minkowski functionals W_ν for randomly distributed balls of radius r(Poisson distribution). For low densities $n = 4\pi/3r^3\rho$ typical configurations are isolated balls with a positive mean Euler characteristic w_3 and a vanishing mean covered volume w_0. For high densities almost the whole space is covered and only isolated cavities remained yielding a positive w_3 if the volume tends to 1 for complete coverage. For intermediate densities the Euler characteristic is negative indicating net-like structures.

In Fig. 4 we show the mean values of the Minkowski functionals per unit volume where we used the original normalization $w_\nu(\rho) = \langle W_\nu \rangle = (\omega_\nu \omega_d / \omega_{d-\nu}) \, m_\nu(\rho)$, for monodispersed balls of radius r in three dimensions. They can be written as functions of the normalized density $n = (4\pi/3) r^3 \rho$

$$w_0(\nu) = 1 - \mathrm{e}^{-n} ,$$

$$
\begin{aligned}
r w_1(n) &= n\,\mathrm{e}^{-n}\,, \\
r^2 w_2(n) &= (n - \frac{3\pi^2}{32} n^2)\,\mathrm{e}^{-n}\,, \\
r^3 w_3(n) &= (n - 3n^2 + \frac{3\pi^2}{32} n^3)\,\mathrm{e}^{-n}\,.
\end{aligned} \tag{3.10}
$$

For monodispersed discs of radius r in two dimension one obtains the mean values

$$
\begin{aligned}
w_0(\nu) &= 1 - \mathrm{e}^{-n}\,, \\
r w_1(n) &= n\,\mathrm{e}^{-n}\,, \\
r^2 w_2(n) &= (n - n^2)\,\mathrm{e}^{-n}
\end{aligned} \tag{3.11}
$$

with the normalized density $n = \pi r^2 \rho$. In the next section we use these results, in particular the mean values of the Euler characteristic, namely $w_3(n)$ in Eq. (3.10) and $w_2(n)$ in Eq. (3.11), to estimate the percolation threshold of the Boolean grain model.

4. Applications

4.1. Porous media

For practical purposes it is important to have a reliable estimate of the percolation threshold for porous media in terms of the shape of the pores. We observe by comparison with numerical data that, at least for certain grain shapes, the mean Euler characteristic vanishes at a density close to the threshold of continuum percolation. In passing we mention, that there is a natural way to formulate a discrete integral geometry for polyhedral sets on regular lattices [14]. The mean Euler characteristics of lattice sets $w_d(p)$ are polynomials in $p = 1 - \mathrm{e}^{-n}$, which coincide with the matching polynomials known from percolation theory [15]. Moreover, $w_2(p)$ vanishes at the exact threshold value p_c for percolation on a two-dimensional self-matching lattice. In the case of continuum percolation, exact values of p_c are not known but some efforts have been made [16–18], based on numerical estimates and excluded-volume arguments, to infer empirical bounds on p_c. Motivated by these attempts to arrive at practically useful percolation criteria, we looked for a possible connection between n_c of continuum percolation and the zeros $n_0^{(d)}$ of $w_d(n)$ [10]. In Table I, numerical n_c-data for some grain shapes are compared with the zeros

$$
n_0^{(2)} = \frac{4\pi f}{u^2}\,, \tag{4.1}
$$

$$
n_0^{(3)} = \frac{48hv}{\pi^2 s^2}[1 - (1 - \frac{\pi^3 s}{6h^2})^{1/2}]\,, \tag{4.2}
$$

obtained from Eqs (3.10) and (3.11); $n_0^{(3)}$ denotes the smallest of the two zeros of $w_3(n)$. The data tempted us to speculate that $n_0^{(2)} \leq n_c^{(2)}$ and $n_0^{(3)} \geq n_c^{(3)}$ might possibly hold as universal bounds for n_c. As a further support for this conjecture, we plotted in Fig. 5 $\rho_c(l)$-values for randomly located and orientated cylinders of length l and fixed radius r in comparison with $\rho_0(l)$, which tends to $2/(\pi r l^2)$ for $l/r \to \infty$. It would be interesting to check whether the second zero of $w_3(n)$ concurs with void percolation, but we are not aware of simulation data for this case.

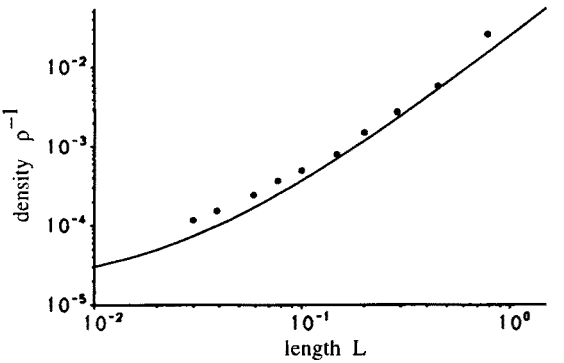

Fig. 5. Percolation threshold $\rho_c(L)$ (black dots, Ref. [18]) for randomly oriented and located cylinders of length L and fixed radius r in comparison with $\rho_0(L)$ (full line). The zero ρ_0 of the Euler characteristic as function of the density is a quite accurate estimate of the percolation threshold ρ_c. This estimate can be calculated explicitly in terms of the morphology of the single shape, namely the cylinder (see Eqs (2.22) and (4.2)).

TABLE I

Threshold values for the percolation density parameter and zeros of the Euler characteristic. The sticks in $d = 2$ are rectangles of length l and vanishing breadth. The discs in $d = 3$ are cylinders of radius $r = 0.5$ and vanishing height. The simulation data are from Ref. [17]: a, Ref. [19]: b.

$d = 2$ discs	$d = 2$ sticks	$d = 3$ balls	$d = 3$ discs
$n_c = 1.12^{a}$	$l^2\rho_c = 5.7^{a}$	$n_c = 0.34^{a}$	$\rho_c = 0.19^{b}$
$n_0 = 1$	$l^2\rho_0 = \pi$	$n_0 = 0.38$	$\rho_0 = 0.22$

4.2. Chemical reaction-diffusion patterns

In order to apply the Minkowski functionals to chemical patterns generated in a diffusion-reaction system we consider Turing-type spatial patterns in a 2-dimensional open spatial reactor with a Chlorite-Iodide-malonic acid reaction. The experiments are described in detail in Ref. [4]. The patterns form in a thin, quasi 2-dimensional disk filled with polyacrylamide gel which prevents convection but allows diffusion of chemicals. Depending on the concentration of Iodide I_3^- the system changes color from yellow to blue which is measured in digitized grey-scale images. Above critical values of the control parameters, namely temperature and reagent concentrations, spatial patterns spontaneously emerge from a spatially homogeneous system. Three different types of patterns are reported in Ref. [4], a hexagonal structure of isolated dots, a lamellar stripe structure broken up into domains of different orientations, and a structure of turbulent stripes, which change shape and orientation much faster than the usual moving of grain boundaries. Such a turbulent pattern is shown in Fig. 1(b). The grey tones of the image correspond to the amount of the oxidized state in the system, *i.e.* inversely proportional to the concentration of Iodide I_3^-. Each image consists of a 512×480 array of pixels with 256 grey levels.

In this section we introduce the concept of iso-density contours of such spatial patterns, *i.e.* thresholds in the grey level, and define the Minkowski functionals for digital images, namely for arrays of pixels.

4.2.1. Thresholding

In order to study the concentration profile in greater detail we introduce a threshold variable $\rho_{\text{th}} = 0, \ldots, 255$ and reset the grey value at each pixel to either white or black depending on whether the original value is larger or lower than ρ_{th}, respectively. Here, white corresponds to high values of the gray-level. In this way we get 256 black-and-white pictures out of one gray-level picture. The qualitative features of the images varies drastically when the threshold parameter ρ_{th} is changed. For high thresholds ρ_{th} we study the regions of maximum concentration, *i.e.* we obtain information concerning the shape of the peaks in the profile. For low thresholds we study the deep valleys of the concentration profile and for intermediate ρ_{th} we obtain more or less the same visual impression as from the gray-scale pattern. Thus the spatial information we get depends strongly on the threshold we set.

4.2.2. Discretizing

Most of the patterns one can obtain from computer simulations or even from observations exhibit a pixel structure which is normally not visible in the continuous spatial structures on a mesoscopic scale. This lattice struc-

ture arise either from the discretization of kinetic equations or from the resolution of digital visual recording equipments like video cameras. Although the picture in Fig. 1 seems to show a continuous pattern, namely smooth boundary lines between black and white areas, it actually consists of a square-lattice of pixels as shown in Fig. 6. Thus, each pixel has exactly four nearest neighbor pixels along the sides of the unit-squares of the lattice and also four next-nearest neighbors connecting the diagonals of the unit-squares. What appears at the beginning to be a disadvantage can be used to calculate morphological measures very fast and accurately. In order to avoid a somewhat arbitrary definition of continuous boundary lines on a scale larger than the pixel size, we define the Minkowski functionals right at the well-defined pixel-level.

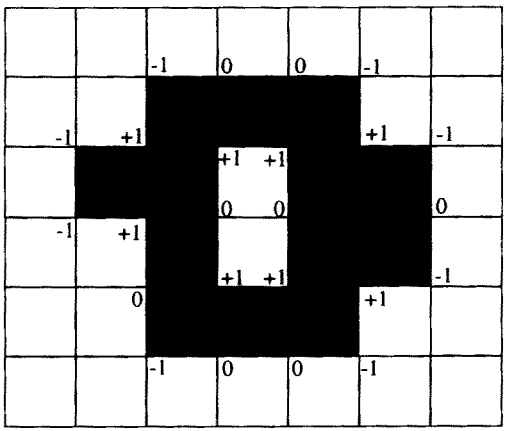

Fig. 6. An array of quadratic pixels is quite often the underlying spatial structure for simulations as well as for experimental data obtained from digital recording equipments like video cameras. Although the boundary length U does not converge to the continuous boundary length for a vanishing lattice spacing, it is convenient to use this lattice structure to calculate the Minkowski measures. One can define an analogue discrete quantity U to the continuous boundary length using the number of edges between black and white pixels on the lattice ($U = 24$ for the configuration above). The area F is given by the number of white pixels ($F = 29$) and the Euler characteristic χ by the sum of curvature variables $\tau \in \{-1, 0, +1\}$ ($\chi = 8(+1) + 8(0) + 8(-1) = 0$).

For instance, the white area of a thresholded black-and-white picture can be obtained simply by counting the number N_ρ of white pixels which depends on the threshold ρ_{th}. The area fraction $F(\rho_{\text{th}}) = N_\rho/N$, normalized by the total number of pixel N, decreases from one to zero by increasing the threshold ρ_{th}.

Although the boundary length of the discretized pattern does not converge to the continuous boundary length for a vanishing lattice spacing, one can define an analogue quantity on the lattice using the number of edges between black and white pixels. Thus, the length of the boundary line $U(\rho_{\text{th}}) = B_\rho/N$ between black and white regions is defined as the number of pairs of neighbored black and white pixels B_ρ normalized by the total number of pixels N. As expected the boundary length U starts at zero for the totally white image at $\rho_{\text{th}} = 0$, increases, reaches a maximum value where the black and white areas are nearly equal, decreases, and finally ends at zero again for the complete black image at $\rho_{\text{th}} = 255$.

In contrast to the surface area F and the line length U the Euler characteristic χ describes the pattern in a purely topological way, *i.e.* without referring to any kind of metric. It measures the connectivity of the black and white regions. Despite this global characterization of the pattern the Euler characteristic can be calculated in a local way. Consider for example one of the four corners of a black pixel and its three neighbored pixels joining at this corner as it is shown in Fig. 6. We define at each corner of a black pixel the 'local curvature' $-1, 0$, or $+1$ depending on the bending of the boundary, *i.e.* $\tau = \pm 1$ if the boundary is curved or $\tau = 0$ iff it continues in a straight line. The sign depends on the orientation of the curvature. Then, the Euler characteristic $\chi = \sum_c \tau_c$ is given by the sum of these curvature variables $\tau_c \in \{-1, 0, +1\}$ at each corner c along the boundary (compare with Eq. 2.5). Thus χ/U describes the mean curvature of the boundary between black and white domains.

4.2.3. Results

For each threshold ρ_{th} and each pattern reported in Ref. [4] we calculated (see Ref. [20]) the white area F, the length U of the boundaries, and the integral of the curvature along the boundaries, *i.e.* the Euler characteristic χ. In particular, we analyzed each pattern indicated by the 'phase diagram' in Fig. 10 of Ref. [4] to study transitions of patterns.

Surprisingly it turns out that there are simple combinations of the quantities $F(\rho_{\text{th}})$, $U(\rho_{\text{th}})$, and $\chi(\rho_{\text{th}})$, namely

$$\begin{aligned} p_F(\rho_{\text{th}}) &= \tanh^{-1}(2F - 1)\,, \\ p_U(\rho_{\text{th}}) &= \frac{U}{F(1-F)} = 4\, s\, \cosh^2\left(p_F(\rho_{\text{th}})\right)\,, \\ p_\chi(\rho_{\text{th}}) &= \frac{\chi}{U}\,, \end{aligned} \tag{4.3}$$

such that the experimental data (considered as functions of the threshold ρ_{th}, which is normalized to the interval $[-1, 1]$ for convenience) may be described

quite well by polynomials of very low order, *i.e.*

$$p_\chi(\rho_{\rm th}) \approx p_\chi^{(0)} + p_\chi^{(1)}\,\rho_{\rm th} + p_\chi^{(2)}\,\rho_{\rm th}^2 + p_\chi^{(3)}\,\rho_{\rm th}^3 \tag{4.4}$$

and which approximate the functions $p_F(\rho_{\rm th})$, $p_U(\rho_{\rm th})$, and $p_\chi(\rho_{\rm th})$ very accurately. This holds for all the patterns reported in Ref. [4]. That is, these special combinations of F, U, and χ may be described by a few parameters $p_\chi^{(\nu)}$, $\nu = 0, 1, 2, 3$ for different patterns and they are in this sense universal in character.

In Fig. 7 we show for an hexagonal pattern (full lines), a lamellar stripe structure (dashed), and a turbulent state (dash-dotted), the function $p_\chi(\rho_{\rm th})$. The lines are the best fits to the data (symbols), which can hardly be distinguished from the experimental data. The coefficients for the polynomials shown in Fig. 7 are given in Table II to illustrate typical values. It was not possible to fit the data curves with polynomials of lower orders than the cubic we used in the ansatz. Higher orders were not needed to improve the accuracy. The coefficients $p_\chi^{(i)}$ $(i = 1, \ldots, 4)$ depend on the control parameters as for instance the concentration of malonic acid or the temperature, but they are reproducible by unchanged experimental conditions. Moreover the fits are not only satisfying sufficient accuracy at intermediate thresholds

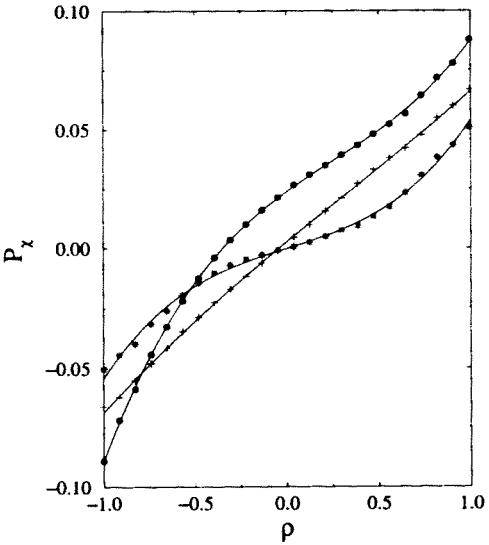

Fig. 7. The mean curvature $P_\chi(\rho_{\rm th}) := \chi/U$ as function of the threshold $\rho_{\rm th}$ turns out to be a cubic polynomial for hexagonal patterns (circles), a linear function for turbulent patterns (plus), and a symmetric cubic polynomial without a quadratic term for stripe patterns (stars).

near zero but also at the very ends, where only few isolated components remain in the images.

TABLE II

Typical values for the coefficients $p_\chi^{(\nu)}$ of the polynomials $p_\chi(\rho_{\rm th})$ for hexagonal, stripe, and turbulent patterns. Coefficients which are at least one order of magnitude smaller than the dominant terms are set in parentheses to illustrate the apparent symmetry of the polynomials.

pattern type	$p_\chi^{(0)}$	$p_\chi^{(1)}$	$p_\chi^{(2)}$	$p_\chi^{(3)}$
hexagons	0.024	0.056	-0.025	0.033
stripes	(-0.00020)	0.024	(-0.000013)	0.031
turbulent	(0.0026)	0.063	(-0.0039)	(0.0044)

The first result of this integral geometric method for pattern analysis is that the area F of the white domains as a function of the threshold $\rho_{\rm th}$ is given mainly by an hyperbolic tangent profile and that the boundary length U is proportional to the product $F(1-F)$, *i.e.* to the product of the areas of black and white components, respectively.

The second even more important result is that the dependence on the experimental conditions like the concentration of malonic acid is reflected only in a finite number of coefficients $p_\mu^{(i)}$. The functional form of the measures F, U, and χ remains the same, *i.e.* it is given always by polynomials of low order.

The third and most striking result is the dependence of the coefficients on the control parameters. For instance, we show in Fig. 8 for seven different concentrations $[H_2SO_4]_0^B$ (mM) at constant $[ClO_2^-]_0^A = 20$ mM the experimental curve $p_\chi(\rho_{\rm th})$ and the best fit using a cubic polynomial. The other control parameters were fixed at the values given for Fig. 10 of Ref. [4]. The shape of the polynomial $p_\chi(\rho_{\rm th})$ indicates a transition from hexagonal point patterns (full lines at $[H_2SO_4]_0^B = 17, 28, 45$, and 100 mM to turbulent structures (dash-dotted lines at $[H_2SO_4]_0^B = 2, 5, 10$ mM). For all turbulent patterns the polynomial is nearly a straight line with no constant, quadratic, or cubic term and therefore shows a zero at $\rho_{\rm th} = 0$. In contrast, for the hexagons these terms cannot be neglected, especially the quadratic term that yields an asymmetry in the functional form of the threshold $\rho_{\rm th}$. The similarity to the symmetry breaking mechanism at thermodynamic phase transitions is obvious, although the physical connection has not been made yet. The transition seems to be continuous with steadily decreasing cubic and quadratic terms in the polynomial. They remain almost zero for the turbulent patterns despite the change in the control parameters. The inset shows the coefficient $p_\chi^{(0)}$ of the polynomial $p_\chi(\rho_{\rm th})$, *i.e.* its value at $\rho_{\rm th} = 0$, as a function of the concentration $[H_2SO_4]_0^B$ (mM). A similar

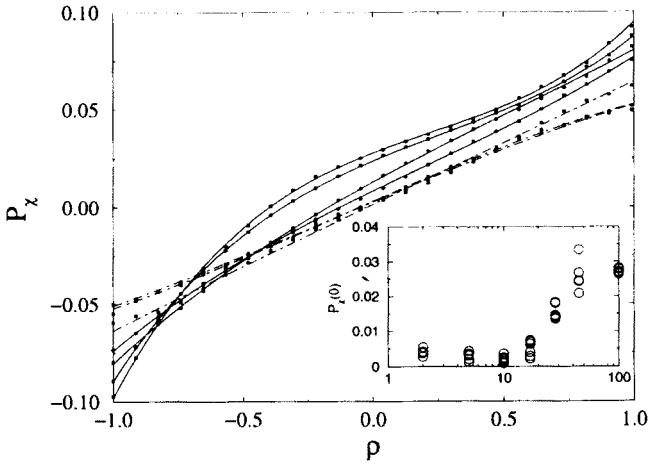

Fig. 8. The polynomial $p_\chi(\rho_{\rm th})$ indicates a transition from hexagonal point patterns (full lines) to turbulent structures (dash-dotted) as a function of $[H_2SO_4]_0^B$ (mM) at constant $[ClO_2^-]_0^A = 20$ mM. The other control parameters were held fixed at the values given for Fig. 10 of Ref. [4]. The transition seems to be continuous with decreasing cubic and quadratic terms in the polynomial. They remain zero for the turbulent patterns. As in Fig. 7 the lines are best fits to the experimental data (black dots). The inset shows the coefficient $p_\chi^{(0)}$ of the polynomial $p_\chi(\rho_{\rm th})$, *i.e.* its value at $\rho_{\rm th} = 0$, as a function of the concentration $[H_2SO_4]_0^B$ (mM).

symmetry breaking in the polynomial is observed for the transition from stripe to turbulent patterns. But the transition seems to be discontinuous. *i.e.* shows a sharp jump in the shape of the polynomial when the type of pattern changes from a turbulent state to stripes.

Relating to these results we want to focus on three questions:

Why is the white area essentially a hyperbolic tangent profile in the threshold $\rho_{\rm th}$? Despite the occurrence of this profile in such diverse fields as thermal statistics of a paramagnet, the width of a fluid interface or the mean-field solution of a ϕ^4-field theory, the connection to the reaction-diffusion system is not clear yet.

Why are the measures $p_F(\rho_{\rm th})$, $p_U(\rho_{\rm th})$, and $p_\chi(\rho_{\rm th})$ finite polynomials in the threshold $\rho_{\rm th}$? They do not need do be that. However, in many models for statistical geometries like the Boolean grain model considered in Sec. 3, similar polynomial behaviors of the Minkowski functional do occur. But what is the underlying statistical model in this case, if there is one?

Why is there a symmetry breaking in the mean curvature, *i.e.* in the Euler characteristic as a measure for the topology of patterns? Is it possible

to formulate a mesoscopic theory of pattern-transitions in analogy to the Landau-theory of thermodynamic phase transitions?

The primary conclusion of this section is that Minkowski functionals, in particular the Euler characteristic, describe quantitatively irregular spatial patterns and their transitions in a morphological way and might be capable of classifying pattern transitions in a similar way like thermodynamic phase transitions.

4.3. Spinodal decomposition

Spinodal decomposition kinetics [21,22] has been a subject of considerable attention in recent years. Particular effort has been focused on identifying scaling regimes using appropriate computer simulation techniques (molecular dynamics [23], Langevin models [24], lattice gas [25] or lattice Boltzmann models [26,27]).

The usual approaches to the characterization of the evolution of the single-phase domains which arise after quenching are mainly based on the time dependent mean domain size $R(t)$ which may be calculated from the first zero of the radial distribution function or from the first moment of the structure factor [28]. Besides of being computationally expensive, the mean domain size alone cannot account for the morphology of the rich variety of geometrical shapes of single phase domains which arise after quenching as well as for their connectivity, which also is changing in time. Therefore it is useful to look for a quantitative characterization of the morphology of spatial patterns which allows for a gain in relevant information on the kinetics of many particle systems, especially when these systems undergo phase transitions like spinodal decomposition. In contrast to the radial distribution function, *i.e.* its first zero, the Minkowski functionals are statistical robust measures which makes it possible to extract information even when large fluctuations are present.

The aim of this section is to make an attempt towards the characterization of the time evolution of the morphology of phase separation using the morphological measures introduced in Sec. 2. For this purpose we use a lattice Boltzmann model on a $2D$ hexagonal lattice derived in Refs [26,27] when modelling the isothermal hydrodynamics of a two phase system. Simulations were mainly done on a 1024×1024 lattice using periodic boundary conditions. The particle distribution functions $f_i(\vec{x},t)$ evolve in accordance to the discretized Boltzmann equation

$$f_i(\vec{x}+\vec{e}_i,t+1) - f_i(\vec{x},t) = \Omega_i(\vec{x},t) \tag{4.5}$$

with the unit vectors

$$\vec{e}_i = \{\cos[2\pi(i-1)/6]\,,\ \sin[2\pi(i-1)/6]\}\ . \tag{4.6}$$

The collision term $\Omega_i(\vec{x}, t)$ is linearized introducing the equilibrium distribution functions f_i^{eq}, $i = 0, 1, \ldots 6$, as well as the relaxation time τ

$$\Omega_i = -\frac{1}{\tau}(f_i - f_i^{\mathrm{eq}}) . \tag{4.7}$$

The equilibrium distribution functions $f_i^{\mathrm{eq}}(\vec{x})$ were expanded as power series in the local velocity $\vec{u}(\vec{x})$ and the appropriate coefficients were determined using local conservation of mass and momentum, as well as Galilean invariance and isotropy of pressure tensor [26]. The local particle density is defined by

$$\rho(\vec{x}, t) = \sum_{i=0}^{i=6} f_i(\vec{x}, t) . \tag{4.8}$$

The density $\rho(\vec{x}, t)$ is shown in Fig. 1(c) for the phase-symmetric mean density $\rho = 3.5$ where the limits are $0 \leq \rho \leq 7$. For the state equation of the fluid

$$p = \rho\psi'(\rho) - \psi(\rho) - \kappa\rho\nabla^2\rho - \frac{\kappa}{2}|\nabla\rho|^2 \tag{4.9}$$

we have chosen a van der Waals fluid with the bulk free energy density ψ

$$\psi = \rho T \ln\left(\frac{\rho}{1-\rho b}\right) - a\rho^2 , \tag{4.10}$$

where T is the system temperature and the constant κ defines the strength of the surface tension. Choosing $a = 9/49$, $b = 2/21$, the critical temperature value becomes $T_{\mathrm{c}} = 0.571$. The spinodal densities $\rho_{\mathrm{sp}}^{\pm}$ at temperature $T < T_{\mathrm{c}}$ are defined as the zeros of the equation $\psi''(\rho) = 0$. For $T = 0.55$ one obtains the densities $\rho_{\mathrm{sp}}^{-} = 2.744$ and $\rho_{\mathrm{sp}}^{+} = 4.315$.

Each simulation run was defined by the mean density $\bar{\rho}$, the value of the surface tension constant κ and the value of the relaxation time τ (which also gives the value of the kinematic viscosity $\nu = (2\tau - 1)/8$ [26]). The lattice system was first initialized with a mean density ρ and 1% random fluctuations of the local density $\rho(\vec{x})$ were allowed. After an initialization, the system was released to evolve during 500 preliminary automaton steps at the initial temperature $T_{\mathrm{in}} = 0.580$ above the critical temperature T_{c}. Then the temperature was changed suddenly to the final value $T_{\mathrm{fin}} = 0.550$. From this moment on ($t = 0$), the system was allowed to evolve to its equilibrium state while snapshots were stored at certain time intervals.

We calculate the morphological measures F, U, and χ for the snapshots (one is shown in Fig. 1(c)) in the same way as for the Turing patterns described in Sec. 4.2. Here we are not interested in the dependence on the threshold ρ_{th} but on the time t. After the initial stage the measures no

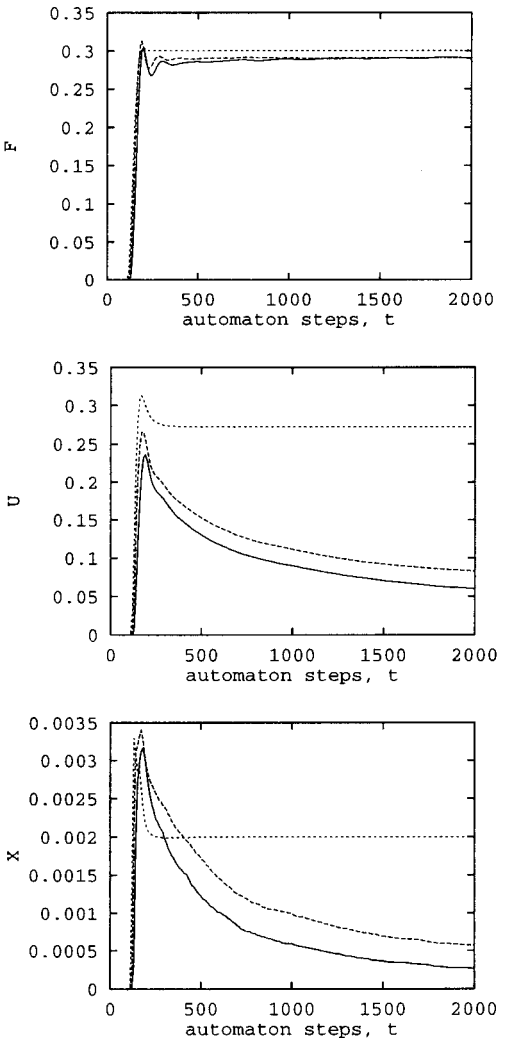

Fig. 9. The time dependent morphological measures F, U, and χ for spinodal decomposition kinetics for $\tau = 0.6$ and different surface stiffness κ (full line $\kappa = 0.01$, dashed $\kappa = 0.005$, and dotted $\kappa = 0.002$). One can clearly distinguish between two different time regime: an early stage spinodal decomposition with increasing measures (in particular U and χ) and a late stage domain growth with decreasing boundary length U and Euler characteristic χ. The maximum values $\bar{U}$ and $\bar{\chi}$ define the transition time $\bar{t}$. For vanishing surface stiffness κ the growth of the domains become extremely slow (see dotted curve).

longer depend significantly on the threshold and we can set it to the mean density value $\rho_{\text{th}} = 3.5$.

In Fig. 9 we show the time dependent morphological measures $F(t)$, $U(t)$, and $\chi(t)$ for an off-symmetric quench with $\rho = 3$ where the fluid phase is the minority phase. One can distinguish between two different time regimes: the early stage of spinodal decomposition kinetics and the late state of domain growth. The growing of density fluctuations leads at early times to the build up of interfaces between homogeneous domains of the coexisting phases. This process is accompanied by an increase of white area F (fluid phase), of the boundary length U of the interface, and of the Euler characteristic due to many disconnected components of the fluid minority phase. In contrast to this early stage, during the late stage domain growth leads to a decrease in the quantities U and χ due to the increase in the characteristic length scale. The area of the fluid phase remains more or less constant and approaches the final value

$$F \sim \frac{\rho - \rho_g}{\rho_l - \rho_g} \quad , \tag{4.11}$$

which is given by the level rule of the coexistence region. The oscillations indicate shape fluctuations of the domains driven by the surface tension and the inertia of the fluid. They are typical initial kinetic phenomena and can be damped by an increase in the viscosity. Because of the demixing of the phases the boundary length $U \to \sqrt{4\pi F}$ and the Euler characteristic $\chi \to 1$ are decaying to the values of a single fluid drop with area F in the vapor phase.

The maximum values $\bar{U}$ and $\bar{\chi}$ mark the transition from the increase during spinodal decomposition and the decrease due to domain growth. Thus, we can use the maximum values to define the transition time $\bar{t}$.

If the inhomogeneous pattern consists of homogeneous domains $\mathcal{A}$ with sharp interfaces the domain growth is due to rearranging the domains without changing the area F of the fluid phase which is given by the level rule in Eq. (4.11). Because the measures $W_\nu(\mathcal{A})$ are homogeneous functions of order $d - \nu$ (see (2.19)) for the normalized quantities we assume the scaling behavior

$$F \sim 1 \quad , \quad U \sim L^{-1} \quad , \quad \chi \sim L^{-2} \tag{4.12}$$

with a scaling length L. We have tested this assumption by changing system parameters such as the surface tension κ and the relaxation time τ and by looking for the same functional behavior of U^2 and χ.

In Fig. 11 we show $U^{-1}(t)$ and $\chi^{-1/2}(t)$, *i.e.* $L(t)$ as function of time. We observe a scaling behavior

$$L(t) \sim t^{\alpha} \tag{4.13}$$

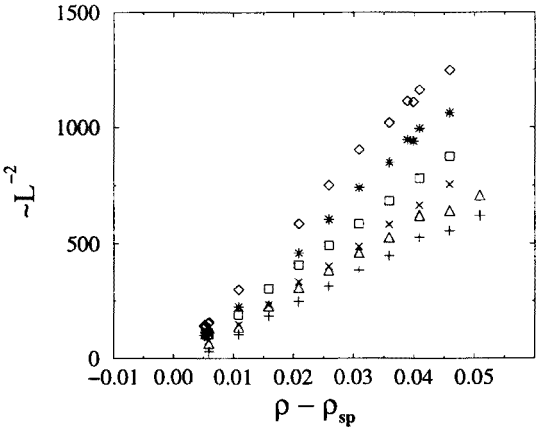

Fig. 10. The maximum values $\bar{U} \sim L^{-1}$ (diamonds $\tau = 0.6$, squares $\tau = 0.7$, triangles $\tau = 0.8$), and $\bar{\chi} \sim L^{-2}$ (stars $\tau = 0.6$, crosses $\tau = 0.7$, plus $\tau = 0.8$) of the morphological measures scale with the characteristic length L. One observes $L \sim (\rho - \rho_{sp})^{-1/2}$ in accordance with Cahn–Hilliard theory of linear stability analysis when approaching the spinodal density ρ_{sp}.

with a scaling exponent α that depends on the relaxation time τ (viscosity). We obtain, for instance, $\alpha = \frac{2}{3}$ for $\tau = 0.54$ and $\alpha = \frac{1}{2}$ for $\tau = 0.8$. For intermediate relaxation times τ we observe a cross over from one scaling to the other, for example, from 2/3 (early times) to 1/2 (late times) at $\tau = 0.6$ (see Fig. 11).

The possibility to distinguish between the early time decomposition and the late stage growth using the definition of the transition time $\bar{t}$ enables us to study the dependence of the scaling length $\bar{L}$ at $\bar{t}$ on the density ρ, in particular when approaching the spinodal density ρ_{sp}. We observe a scaling behavior for the maximum values $\bar{U}$ and $\bar{\chi}$ with the diverging characteristic length scale

$$\bar{L} \sim (\rho - \rho_{sp})^{-1/2}, \tag{4.14}$$

which is shown in Fig. 10. This scaling behavior is consistent with the prediction of the Cahn–Hilliard theory of early time spinodal decomposition [21]. The transition time itself scales in the same way $\bar{t} \sim (\rho - \rho_{sp})^{-1/2}$ indicating a density independent mean velocity $\bar{L}/\bar{t}$ of the fluid particles during the early stage, which depends only on the temperature T.

Finally, we want to emphasize that the calculation of the morphological measures is convenient and fast since one has to count only pixels. The definition and calculation of the characteristic length scale by using the scaling of the morphological measures U and χ instead of the correlation function

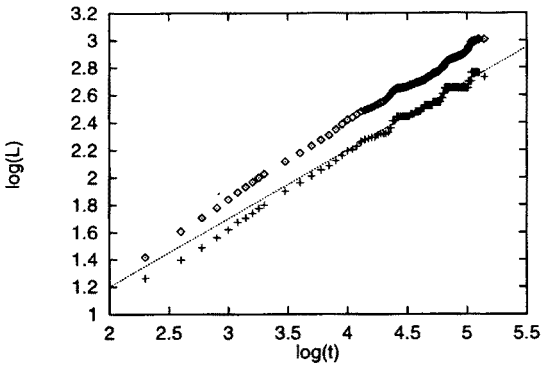

Fig. 11. In the late stage of spinodal decomposition kinetics (long times) one finds the scaling behavior $U \sim L^{-1}$ (plus), and $\chi \sim L^{-2}$ (diamonds) for the morphological measures. We observe the growth law $L \sim t^{\alpha}$ with $\alpha = 1/2$ (dotted line) for $\tau = 0.6$ (diffusive regime).

makes it possible to decrease the computational time of the simulation considerably. Moreover, we obtain an immediate test of the scaling assumption of the morphology during the domain growth and also a clear definition of the early time regime of spinodal decomposition. In other words, Minkowski functionals provide a mean to characterize the cross over from early time spinodal decomposition to the late stage domain growth.

In three dimensions, the morphological measures are a more promising tool since the topology of the patterns changes drastically with the mean density ρ. In particular one finds a whole region of densities between the percolation thresholds as shown in Sec. 1.1 where the pattern is bicontinuous. Since the late stage growth is expected to depend on the topology of the spatial structure the morphological measures may provide a mean to study the dependence of the scaling behavior on the morphology.

5. Summary

We defined morphological measures of d-dimensional patterns as additive (2.1), motion-invariant (2.2) and continuous (2.3) functionals of the spatial domains. The theorem (2.29) asserts that a morphological measure can be represented as a sum of $d + 1$ Minkowski functionals W_ν defined by the Eqs (2.11). The Minkowski functionals are familiar geometric quantities, in particular, for $d = 3$ the Euler characteristic χ, the covered volume V, the surface area S of the coverage, and its integral mean curvature H. The principal kinematical formulae (2.30) provide means to calculate mean values (3.9) of the Minkowski functionals for the Boolean grain model where

random structures in space are generated by overlapping grains (balls, sticks) each with arbitrary location and orientation. We applied the concept of integral geometry and in particular the notion of morphological measures to the following physical systems:

(A) Porous media can be generated by the Boolean grain model, *i.e.* by overlapping sets of arbitrary shape distributed uniformly in space. The percolation threshold of such porous media can be estimated accurately by Eqs (4.1) and (4.2) in terms of the shape, namely volume, surface area, integral mean curvature, and Euler characteristic of the distributed pores.

(B) Turing patterns observed in chemical reaction-diffusion systems can be analyzed in terms of the morphological measures, which turn out to be cubic polynomials in the grey-level of the patterns. Thus the dependence on the experimental conditions is reflected only in a finite number of coefficients, which can be used as order parameters for the morphology of the patterns. We observe a symmetry-breaking of the polynomials when the type of the pattern changes. Therefore, it is possible to describe the pattern-transitions quantitatively and it may be possible to classify them in a similar way to thermodynamic phase transitions.

(C) Integral geometry provides means to study the morphology of homogeneous phases during spinodal decomposition. We observe the scaling behavior (4.12) of the Minkowski functionals W_ν defining a typical length scale L. Morphological measures are convenient and fast to calculate during the time evolution yielding accurate values of the scaling exponent α for various hydrodynamic regimes (see Eq. (4.13)). Additionally, it is possible to define the cross over from the early stage decomposition to the late stage growth and to analyze the morphology of decomposition patterns at early times. In particular, for early times (decomposition regime) we recover the scaling behavior (4.14) predicted by the Cahn–Hilliard theory when approaching the spinodal density. In contrast to the radial distribution function, *i.e.* its first zero, the Minkowski functionals are statistical robust measures which makes it possible to extract the length scale L even when large fluctuations are present.

Minkowski functionals are useful geometric measures to describe patterns and to gain relevant information on physical phenomena related to the morphology of the spatial structure.

My thanks for discussions and cooperation go to H. Wagner, H. Swinney, and V. Sofonea. The simulations of the spinodal decomposition were carried out on the CM-5 parallel machine at BUGH Wuppertal by V. Sofonea.

REFERENCES

[1] H. Reiss, *J. Phys. Chem.* **96**, 4736 (1992).

[2] F.A.L. Dullien, *Porous Media, Fluid Transport and Pore Structure*, Academic Press, San Diego 1992.

[3] A.M. Turing, *Phil. Trans. R. Soc. London Ser. B* **327**, 37 (1952).

[4] Q. Ouyang, H.L. Swinney, *Chaos* **1**, 411 (1991).

[5] H. Hadwiger, *Vorlesungen über Inhalt, Oberfläche und Isoperimetrie*, Springer Verlag, 1957.

[6] L.A. Santalò, *Integral Geometry and Geometric Probability*, Addison–Wesley, Reading, MA 1976.

[7] W. Weil, *Stereology*, in: *Convexity and its Applications*, eds P.M. Gruber, J.M. Wills, Birkhäuser 1983.

[8] A. Rosenfeld, A.C. Kak, *Digital Picture Processing*, Academic Press, New York 1976.

[9] J. Serra, *Image Analysis and Mathematical Morphology*, Vol.1,2 Academic Press, 1982.

[10] K.R. Mecke, H. Wagner, *J. Stat. Phys.* **64**, 843 (1991).

[11] D. Stoyan, W.S. Kendall, J. Mecke, *Stochastic Geometry and its Applications* Wiley & Sons, 1987.

[12] E.F. Harding, D.G. Kendall, *Stochastic Geometry*, 1974.

[13] G. Matheron, *Random Sets and Integral Geometry*, 1975.

[14] K. R. Mecke, *Integralgeometrie in der Statistischen Physik*, Ph.D. thesis (in German), Ludwig–Maximilians Universität, München, 1993: *Reihe Physik* Vol. 25, Verlag Harri Deutsch, Frankfurt 1994.

[15] M.F. Sykes, J.W. Essam, *J. Math. Phys.* **5**, 1117 (1964).

[16] H. Scher, R. Zallen, *J. Chem. Phys.* **53**, 3759 (1970).

[17] G.E. Pike, C.H. Seager, *Phys. Rev.* **B10**, 1421 (1974).

[18] I. Balberg, *Phil. Mag.* **B56**, 991 (1987).

[19] E. Charlaix, *J. Phys. A: Math. Gen.* **19**, L533 (1986).

[20] K.R. Mecke, *Phys. Rev.* **E53**, 4794 (1996).

[21] J.D. Gunton, M. Miguel, P.S. Sahni, in *Phase Transition and Critical Phenomena* Vol. 8, eds C. Domb and J.L. Lebowitz, Academic Press, New York 1983.

[22] A.J. Bray, *Adv. Phys.* **43**, 357 (1994).

[23] E. Velasco, S. Toxvaerd, *Phys. Rev.* **E54**, 605 (1996).

[24] T. Lookman, Y. Wu, F.J. Alexander, S. Chen, *Phys. Rev.* **E53**, 5513 (1996).

[25] D.H. Rothman, S. Zaleski, *Rev. Mod. Phys.* **66**, 1417 (1994).

[26] M.R. Swift, W.R. Osborn, J. M. Yeomans, *Phys. Rev. Lett.* **75**, 830 (1995).

[27] W.R. Osborn, E. Orlandini, M.R. Swift, J.M. Yeomans, J.R. Banavar, *Phys. Rev. Lett.* **75**, 4031 (1995).

[28] M.P. Allen, D.J. Tildesley, *Computer Simulation of Liquids*, Oxford University Press, Oxford 1993.